Advances in Materials Research, *Vol. 13, No. 2 (2024) 87-102*
https://doi.org/10.12989/amr.2024.13.2.087

Multilayered viscoelastic beam loaded in torsion under strain-path control: A delamination analysis

Victor I. Rizov*

Department of Technical Mechanics, University of Architecture, Civil Engineering and Geodesy, 1 Chr. Smirnensky blvd., 1046 - Sofia, Bulgaria

(*Received March 16, 2023, Revised June 20, 2023, Accepted June 21, 2023*)

Abstract. This paper is focused on the delamination analysis of a multilayered beam structure loaded in torsion under strain-path control. The beam under consideration has a rectangular cross-section. The layers of the beam are made of different viscoelastic materials which exhibit continuous inhomogeneity in longitudinal direction. Since the delamination is located inside the beam structure, the torsion moments in the two crack arms are obtained by modeling the beam as an internally static undetermined structure. The strain energy stored in the beam is analyzed in order to derive the strain energy release rate (SERR). Since the delamination is located inside the beam, the delamination has two tips. Thus, solutions of the SERR are obtained for both tips. The solutions are verified by analyzing the beam compliance. Delamination analysis with bending-torsion coupling is also performed. The solutions derived are time-dependent due to two factors. First, the beam has viscoelastic behavior and, second, the angle of twist of the beam-free end induced by the external torsion moment changes with time according to a law that is fixed in advance.

Keywords: delamination; inhomogeneous material; multilayered beam structure; torsion; viscoelastic behavior

1. Introduction

The best choice of material for a given engineering structure depends largely on the loading conditions. If these conditions are different in different parts of the structure, a continuously inhomogeneous structural material is a very good candidate for replacement of the conventional homogeneous materials used traditionally in various areas of engineering. The continuously inhomogeneous materials are particularly attractive because of the fact that their material properties vary smoothly along one or more directions in the solid. A very popular type of continuously inhomogeneous material is the functionally graded material (FGM) (Akbulut and Sonmez 2008, Akbulut *et al.* 2020, Butcher *et al.* 1999, Gasik 2010, Hedia *et al.* 2014). As a matter of fact, FGM-s can be defined as continuously inhomogeneous composites made of two or more constituent materials (Chen *et al.* 2020, Hirai and Chen 1999, Madan *et al.* 2020, Mahamood and Akinlabi 2017, Markworth *et al.* 1995, Miyamoto *et al.* 1999, Nikbakht *et al.* 2019, Nemat-Allal *et al.* 2011, Ridha *et al.* 2016, Saiyathibrahim *et al.* 2019). The FGM-s are fabricated by continuously mixing of their

*Corresponding author, Professor, E-mail: v_rizov_fhe@uacg.bg

http://www.techno-press.org/?journal=amr&subpage=5 ISSN: 2234-0912 (Print), 2234-179X (Online)

constituent materials. The microstructure and the ratios of constituent materials change continuously along definite directions in the structural members (Radhika *et al.* 2020, Shrikantha Rao and Gangadharan 2014, Toudehdehghan *et al.* 2017, Uslu Uysal and Kremzer 2015, Uslu Uysal and Güven 2015, Uslu Uysal 2016). There are advanced technologies for production of FGM-s which allow for tailoring of material properties in order to meet varied exploitation requirements (Gasik 2010, Mahamood and Akinlabi 2017, Markworth *et al.* 1995, Miyamoto *et al.* 1999).

In principle, a multilayered inhomogeneous structure is defined as a structure consisting of adhesively bonded layers made of different inhomogeneous materials. The number and the thickness of layers may be arbitrary. Various kinds of multilayered structures (beams, plates, columns, panels, shells, etc.) are frequently used in different load-bearing constructions in contemporary engineering (Nguyen *et al.* 2015, Nguyen *et al.* 2020). Multilayered structures arouse great interest in the engineering community. One of the important advantages of multilayered structures is the high strength-to-weight and strength-to-thickness ratio. Therefore, one of the ways for weight savings is to use multilayered materials for the manufacturing of various engineering structures and facilities. Multilayered structures are very useful for engineering applications which are highly sensitive with respect to weight.

The delamination phenomenon is of specific importance for the safety of inhomogeneous structures (Dolgov 2002, 2005, 2016, Uslu Uysal and Güven 2016, Rizov 2022, Rizov and Altenbach 2023, Rizov 2023). In fact, delamination is a failure mode representing the separation of layers which may have a significant effect on structural integrity, reliability and durability. The presence of delamination in multilayered structural members and components causes a reduction of strength and stiffness and exhausts the load-carrying capacity. Also, the delamination increases the risk of collapse of the entire structure.

This paper analyzes delamination of a multilayered inhomogeneous beam structure of a rectangular cross-section subjected to torsion under strain-path control. The need for carrying-out of such analysis is because multilayered beams loaded in torsion are used in many load-caring structural applications. However, the delamination analyses of multilayered systems under torsion are dealing chiefly with beams of circular cross-section (Rizov 2018, 2020, 2021). It should be underlined further that the existing research work in the field of delamination fracture considers beam structures of rectangular cross-section usually subjected to bending. For instance, Hutchinson and Suo (1992) have developed a huge number of analyses of various delamination cases assuming linear-elastic behavior. Solutions of the SERR have been found-out (Hutchinson and Suo 1992). These solutions have been used to investigate the influence of different factors on the delamination behavior (Hutchinson and Suo 1992). Analyses of delamination fracture in multilayered beams of rectangular cross-section under bending have been carried-out by Hsueh *et al.* (2009). The SERR has been derived again for the case of linear-elastic behavior of the multilayered material (Hsueh *et al.* 2009). The existing research work on fracture in continuously inhomogeneous beam structures (like, for instance, functionally graded beams) also deal mainly with beams of rectangular cross-section for the most part subjected to bending. Cracks in functionally graded beams under three-point bending have been analyzed by Carpinteri and Pugno (2006). The beams considered have linear-elastic behavior (Carpinteri and Pugno 2006). Works dealing with fracture of functionally graded materials and structures have been reviewed by Tilbrok *et al.* (2005). The functionally graded structures considered are usually under bending and exhibit linear-elastic mechanical behavior (Tilbrok *et al.* 2005).

Apparently, delamination in multilayered inhomogeneous viscoelastic beams of rectangular

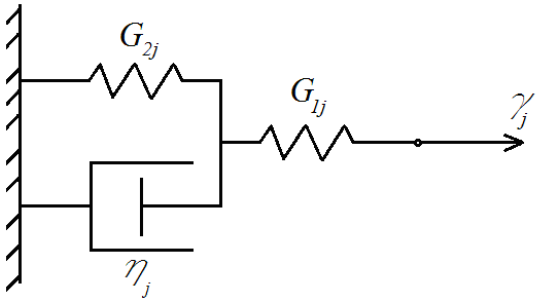

Fig. 1. Viscoelastic mechanical model

cross-section subjected to torsion under strain-path control has been feebly studied up to now. The present paper bridges this gap in the existing research work. The layers of the rectangular viscoelastic beam analyzed in the present paper are continuously inhomogeneous along the length of the beam. Delamination is located between layers inside the beam. The left-hand and right-hand delamination crack arms have different widths. The main purpose of the paper is to obtain the SERR under strain-path control. The present paper is organized in the following way.

1. Describing the viscoelastic model applied for analyzing the mechanical behavior of the beam with a delamination subjected to torsion under strain-path control.
2. Modeling the beam as an internally static undetermined structure.
3. Determining the SERR under strain-path control for both delamination tips.
4. Performing a parametric analysis of the SERR.
5. Determining the SERR with taking into account the bending-torsion coupling.
6. Comparing the outcome of the delamination analysis with bending-torsion coupling with the torsion case alone.
7. Formulating the main conclusions.

One of the major limitations of the theoretical model used in the present delamination study ensues from the fact that the beam structure has to be loaded in torsion (or in torsion and bending) under strain-path control.

2. Beam with delamination loaded in torsion under strain-path control

The viscoelastic mechanical model displayed in Fig. 1 is under strain-path control.

The variation of the shear strain, γ_j, with time, t, is set as

$$\gamma_j = v_j t \tag{1}$$

where v_j is a parameter that controls the variation. The constitutive law of the model in Fig. 1 is written as (Zubchaninov 1990)

$$\tau_j = G_{j*} v_j t + m_j (G_{1j} - G_{j*}) \left(1 - e^{-\frac{t}{m_j}}\right) v_j \tag{2}$$

where

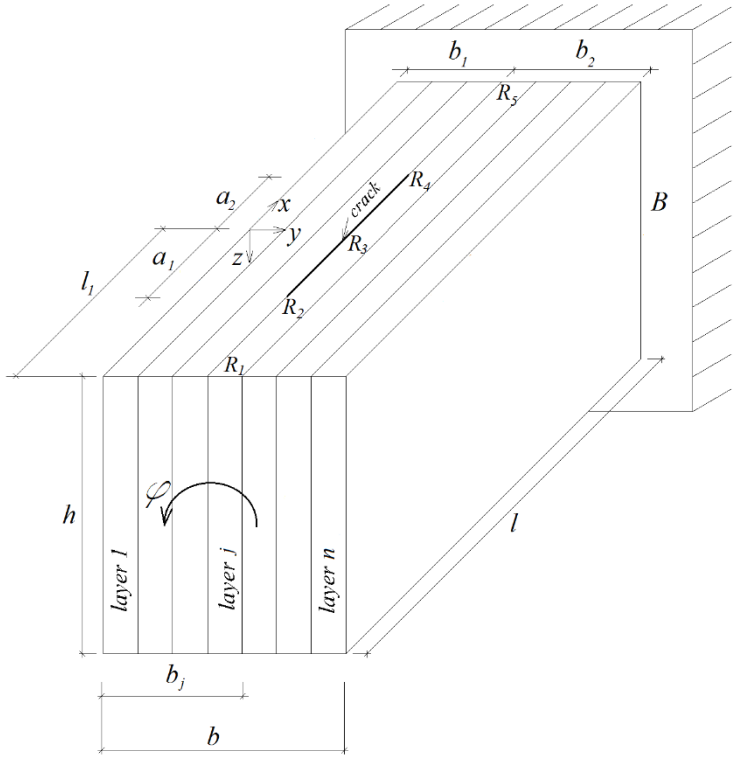

Fig. 2 Multilayered viscoelastic beam structure with a delamination

$$m_j = \frac{\eta_j}{G_{1j} + G_{2j}} \tag{3}$$

$$G_{j^*} = \frac{G_{1j} G_{2j}}{G_{1j} + G_{2j}} \tag{4}$$

In Eqs. (2), (3) and (4), τ_j is the shear stress, η_j is the coefficient of viscosity of the dashpot (Fig. 1), G_{1j} and G_{2j} are the shear moduli of the two springs in the model.

The time-dependent shear modulus of the model in Fig. 1 is found as

$$G_{Dj} = \frac{\tau_j}{\gamma_j} \tag{5}$$

By substituting of Eqs. (1) and (2) in (5), one determines

$$G_{Dj} = G_{j^*} + m_j (G_{1j} - G_{j^*}) \left(1 - e^{-\frac{t}{m_j}} \right) \frac{1}{t} \tag{6}$$

The time-dependent shear modulus Eq. (6) is used for modeling the viscoelastic behavior of the beam structure displayed in Fig. 2. The beam is rectangular with width, b, and thickness, h. The length of the beam is l. The beam is with longitudinal viscoelastic layers of different widths. The materials of the layers are different. There is a delamination crack between layers as displayed in Fig. 2. The length of the crack is denoted by a_1+a_2. The widths of crack arms are b_1 and b_2 (Fig. 2). The beam is clamped in section, B. The beam is loaded in torsion at its free end so as the angle of twist, φ, varies with time according to the following law (Fig. 2)

$$\varphi = v_{\varphi} t \tag{7}$$

where v_{φ} is a parameter that controls the variation.

The layers of the beam exhibit continuous material inhomogeneity along the beam length. The following laws are used for describing the variation of the shear moduli and the coefficient of the viscosity of the jth layer in the longitudinal direction

$$G_{1j} = G_{1Hj} + \frac{G_{1Lj} - G_{1Hj}}{l^{\beta_j}} (x + l_1)^{\beta_j} \tag{8}$$

$$G_{2j} = G_{2Hj} + \frac{G_{2Lj} - G_{2Hj}}{l^{\delta_j}} (x + l_1)^{\delta_j} \tag{9}$$

$$\eta_j = \eta_{Hj} + \frac{\eta_{Lj} - \eta_{Hj}}{l^{\psi_j}} (x + l_1)^{\psi_j} \tag{10}$$

where

$$-l_1 \le x \le l - l_1 \tag{11}$$

In Eqs. (8), (9), (10) and (11), G_{1Hj}, G_{2Hj}, η_{Hj}, G_{1Lj}, G_{2Lj} and η_{Lj} the values of G_{1j}, G_{2j} and $\eta_j \eta_j$ at the ends of the beam, β_j, δ_j and ψ_j are parameters which control the variation of material properties, the abscissa, x, is displayed in Fig. 2.

In order to derive the SERR for the delamination crack in the beam under consideration (Fig. 2), the torsion moments in the two crack arms have to be determined first. In fact, the beam represents a structure with one degree of internal static indeterminacy. The moment, T_1, in the left crack arm is treated as internal redundant unknown. The static indeterminacy is resolved by applying the theorem of Menabrea

$$\frac{\partial U}{\partial T_1} = 0 \tag{12}$$

Where U is the strain energy cumulated in the beam. This strain energy is found as

$$U = U_1 + U_2 + U_3 + U_4 \tag{13}$$

where U_1 is the strain energy in portion, R_1R_2 (Fig. 2), U_2 and U_3 are the strain energies in the crack arms, U_4 is the strain energy in portion, R_4R_5.

The strain energy in portion, R_1R_2, is determined as

$$U_1 = \sum_{j=1}^{j=n} \int_{-l_1}^{-a_1} \left(\iint_{(A_j)} u_{01j} dA \right) dx \tag{14}$$

Where n is the number of layers, A_j is the area of the j-th layer, u_{01j} is the density of strain energy in the j-th layer. u_{01j} is found as

$$u_{01j} = \frac{1}{2} \tau_j \gamma_j \tag{15}$$

From Eqs. (5) and (15), one derives

$$u_{01j} = \frac{\tau_j^2}{2G_{Dj}} \tag{16}$$

where τ_j is obtained by applying the following formula for shear stresses in multilayered beam loaded in torsion (Chobanian 1997)

$$\tau_j = \frac{T}{S} \left\{ \left[\sum_{k=1,3,...}^{\infty} \left(P_{k,j} ch\alpha_k y + Q_{k,j} sh\alpha_k y \right) \alpha_k sh\alpha_k z \right]^2 + \right.$$
$$\left. + \left[\sum_{k=1,3,...}^{\infty} \left(P_{k,j} sh\alpha_k y + Q_{k,j} ch\alpha_k y + \frac{8G_{Dj}h^2}{k^3\pi^3} \right) \alpha_k \cos\alpha_k z \right]^2 \right\}^{\frac{1}{2}} \tag{17}$$

where S is the stiffness in torsion of the beam, T is the torsion moment (T is unknown quantity). The quantity, α_k, is found as

$$\alpha_k = \frac{k\pi}{h} \tag{18}$$

The axes, y and z, are displayed in Fig. 2. The quantities, $P_{k,j}$ and $Q_{k,j}$, are determined by using the following recurrent formulae (Chobanian 1997)

$$P_{k,j} = \frac{2}{(g_{j,j+1} - 1) sh2\alpha_k b_j} \left[Q_{k,j+1} g_{j,j+1} + Q_{K,j} \left(sh^2\alpha_k b_j - g_{j,j+1} ch^2\alpha_k b_j \right) + \right.$$
$$\left. + g_{j,j+1} (r_{k,j+1} - r_{k,j}) ch\alpha_k b_j \right] \tag{19}$$

$$P_{k,j+1} = \frac{2}{(g_{j,j+1} - 1) sh2\alpha_k b_j} \left[Q_{K,j+1} \left(ch^2\alpha_k b_j - g_{j,j+1} sh^2\alpha_k b_j \right) - \right.$$
$$\left. - Q_{k,j} + (r_{k,j+1} - r_{k,j}) ch\alpha_k b_j \right] \tag{20}$$

where

$$g_{j,j+1} = \frac{G_{Dj}}{G_{D(j+1)}} \tag{21}$$

$$r_{k,j} = \frac{8G_{Dj}h^2}{k^3\pi^3} \tag{22}$$

In Eqs. (19), (20), (21) and (22), j=1, 2, …, n, n-1. The quantities, b_j, are displayed in Fig. 2. Besides (Chobanian 1997),

$$P_{k,1} = -\frac{Q_{k,1}ch\alpha_k b_0 + r_{k,1}}{sh\alpha_k b_0} \tag{23}$$

$$P_{k,n} = -\frac{Q_{k,n}ch\alpha_k b_n + r_{k,n}}{sh\alpha_k b_n} \tag{24}$$

All unknown quantities, $P_{k,j}$ and $Q_{k,j}$, with the same index, k, are determined consecutively by using Eqs. (19), (20), (23) and (24).

The stiffness, S, that is involved in Eq. (17), is found as (Chobanian 1997)

$$S=\frac{8}{\pi^2}\sum_{k=1,3,\ldots}^{\infty}\frac{1}{k^2}\left\{\frac{\alpha_k}{2}\sum_{j=1}^{n} r_{k,j}\left(b_j - b_{j-1}\right) + +\sum_{j=1}^{n} P_{k,j}sh\frac{\alpha_k\left(b_j + b_{j-1}\right)}{2}sh\frac{\alpha_k\left(b_j - b_{j-1}\right)}{2} + \right.$$
$$\left. +\sum_{j=1}^{n} Q_{k,j}sh\frac{\alpha_k\left(b_j - b_{j-1}\right)}{2}ch\frac{\alpha_k\left(b_j + b_{j-1}\right)}{2}\right\} \tag{25}$$

By substituting of Eqs. (17) in (16), one obtains

$$u_{01j} = \frac{T^2\lambda_{1j}}{2G_{Dj}} \tag{26}$$

where

$$\lambda_{1j} = \frac{1}{S^2}\left\{\left[\sum_{k=1,3,\ldots}^{\infty}\left(P_{k,j}ch\alpha_k y + Q_{k,j}sh\alpha_k y\right)\alpha_k sh\alpha_k z\right]^2 + \right.$$
$$\left. +\left[\sum_{k=1,3,\ldots}^{\infty}\left(P_{k,j}sh\alpha_k y + Q_{k,j}ch\alpha_k y + \frac{8G_{Dj}h^2}{k^3\pi^3}\right)\alpha_k\cos\alpha_k z\right]^2\right\} \tag{27}$$

The strain energy, U_2, is found as

$$U_2 = \sum_{j=1}^{j=n_1}\int_{-a_1}^{a_2}\left(\iint_{(A_j)} u_{02j}dA\right)dx \tag{28}$$

where n_1 is the number of layers in this crack arm, A_j is the area of the j-th layer, u_{02j} is the strain energy density in the j-th layer. u_{02j} is derived as

$$u_{02j} = \frac{T_1^2\lambda_{2j}}{2G_{Dj}} \tag{29}$$

where λ_{2j} is obtained by replacing of S with S_1 in Eq. (27). The stiffness in torsion, S_1, of the left-hand crack arm is determined by replacing of n with n_1 in Eq. (25).

The strain energy stored in the right-hand crack arm is calculated as

$$U_3 = \sum_{j=1}^{j=n_2} \int_{-a_1}^{a_2} \left(\iint_{(A_j)} u_{03j} dA \right) dx \tag{30}$$

where n_2 is the number of layers, u_{03j} is the strain energy density in the j-th layer. u_{03j} is found as

$$u_{03j} = \frac{T_2^2 \lambda_{3j}}{2G_{Dj}} \tag{31}$$

where T_2 is the torsion moment in the right-hand crack arm, λ_{3j} is obtained by replacing of S with S_2 in Eq. (27). In order to determine the stiffness in torsion, S_2, of the right-hand crack arm, n is replaced with n_2 in Eq. (25). The torsion moment, T_2, is expressed as a function of T_1. For this purpose, the following equation of equilibrium of the torsion moments is used

$$T_1 + T_2 = T \tag{32}$$

By using Eq. (32), Eq. (31) is re-written as

$$u_{03j} = \frac{(T - T_1)^2 \lambda_{3j}}{2G_{Dj}} \tag{33}$$

Finally, the strain energy in the un-cracked beam portion, R_4R_5, is derived as

$$U_4 = \sum_{j=1}^{j=n} \int_{a_2}^{l-l_1} \left(\iint_{(A_j)} u_{04j} dA \right) dx \tag{34}$$

where u_{04j} is obtained by using Eq. (26).

There are two unknowns, T_1 and T, in Eq. (12). Therefore, a further equation with these unknowns is needed. To constitute such an equation, the angle of twist is found by applying the theorem of Castigliano

$$\frac{\partial U}{\partial T} = \varphi \tag{35}$$

After substituting of the strain energy in Eqs. (12) and (35), the two equations are solved with respect to T_1 and T.

First, the SERR, G, is derived at increase of the delamination length at the delamination tip located in section, R_2, of the beam (Fig. 2). The SERR is written as

$$G = \frac{\partial U}{h \partial a_1} \tag{36}$$

By substituting of Eqs. (13), (14), (28), (30) and (34) in (36), one obtains

$$G=\frac{1}{h}\left[\sum_{j=1}^{j=n}\left(-\iint_{(A_j)}u_{01j}dA\right)+\sum_{j=1}^{j=n_1}\left(\iint_{(A_j)}u_{02j}dA\right)+\sum_{j=1}^{j=n_2}\left(\iint_{(A_j)}u_{03j}dA\right)\right] \tag{37}$$

The integration in Eq. (37) is carried-out by the MatLab. Eq. (37) is applied to obtain the SERR at various values of time. It should be mentioned that the material properties involved in Eq. (37) are determined at $x=-a_1$.

The SERR at increase of the delamination length at the delamination tip located in section, R_4, of the beam (Fig. 2) is derived as

$$G=\frac{\partial U}{h\partial a_2} \tag{38}$$

By combining of Eqs. (13), (14), (28), (30), (34) and (36), one obtains

$$G=\frac{1}{h}\left[\sum_{j=1}^{j=n_1}\left(\iint_{(A_j)}u_{02j}dA\right)+\sum_{j=1}^{j=n_2}\left(\iint_{(A_j)}u_{03j}dA\right)-\sum_{j=1}^{j=n}\left(\iint_{(A_j)}u_{04j}dA\right)\right] \tag{39}$$

The MatLab is used to solve the integrals in Eq. (39). The material properties involved in Eq. (39) are found at $x=a_2$. The SERR can be derived at various values of time by Eq. (39).

The compliance of the beam is analyzed in order to determine an alternative solution of the SERR for verification of Eqs. (37) and (39). The compliance, C, is derived as

$$C=\frac{\varphi}{T} \tag{40}$$

The angle of twist is expressed as

$$\varphi=\int_{-l_1}^{-a_1}\frac{T}{S}dx+\int_{-a_1}^{a_2}\frac{T_1}{S_1}\frac{T_1}{T}dx+\int_{-a_1}^{a_2}\frac{T-T_1}{S_2}\frac{T-T_1}{T}dx+\int_{a_2}^{l-l_1}\frac{T}{S}dx \tag{41}$$

Eq. (41) is found by using the integrals of Maxwell-Mohr. The quantities, T_1/T and $(T_1/T)/T$, in Eq. (41) are the moments generated by the unit loading for determination of φ.

The SERR at increase of the delamination length at the delamination tip located in section, R_2, of the beam is written as

$$G=\frac{T^2}{2h}\frac{\partial C}{\partial a_1} \tag{42}$$

By combining of Eqs. (41) and (42), one obtains

$$G=\frac{1}{2h}\left[-\frac{T^2}{S}+\frac{T_1^2}{S_1}+\frac{(T-T_1)^2}{S_2}\right] \tag{43}$$

where the material properties are found at $x=-a_1$. The SERR derived by Eq. (43) match these determined by Eq. (37). This confirms the correctness of the solution of the SERR at increase of

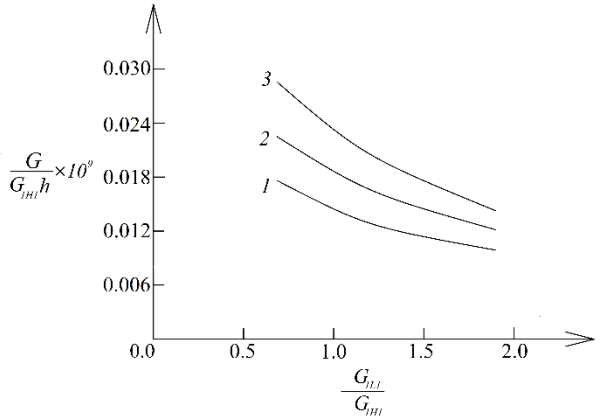

Fig. 3 The SERR presented as a function of G_{1L1}/G_{1H1} ratio (curve 1 - at ν_φ=0.05×10^{-8} *rad/sec*, curve 2 - at ν_φ=0.10×10^{-8} *rad/sec* and curve 3 - at ν_φ=0.15×10^{-8} *rad/sec*)

delamination length at the delamination tip located in section, R_2, of the beam.

The SERR at increase of the delamination length at the delamination tip located in section, R_4, of the beam is found as

$$G = \frac{T^2}{2h}\frac{\partial C}{\partial a_2} \tag{44}$$

By substituting of Eqs. (41) in (44), one derives

$$G = \frac{1}{2h}\left[\frac{T_1^2}{S_1} + \frac{(T-T_1)^2}{S_2} - \frac{T^2}{S}\right] \tag{45}$$

Here, the material properties are obtained at $x=a_2$. The fact that the SERR found by Eq. (45) match these determined by using Eq. (39) verifies the solution of G at increase of delamination length at the delamination tip located in section, R_4, of the beam.

3. Parametric analysis

This section of the paper contains results of a parametric analysis. The results are derived by applying the solutions of the SERR obtained in section 2 of the paper. It is assumed that b=0.030 m, h=0.045 m, l=0.800 m, l_1=0.400 m, n=4, n_1=2, ν_φ=0.15×10^{-8}, *rad/sec*, β_j=0.7, δ_j=0.7 and ψ_j=0.7.

The effect of the variation of G_{11} in layer 1 along the beam length on the SERR is analyzed. For this purpose, the SERR is presented as a function of G_{1L1}/G_{1H1} ratio in Fig. 3 at three values of parameter, ν_φ. It should be specified that the SERR in Fig. 3 is expressed in non-dimensional form as $G_N = G/(G_{1H1}h)$. It is evident from Fig. 3 that when G_{1L1}/G_{1H1} ratio increases, the SERR decreases. One can observe also in Fig. 3 that increase of parameter, ν_φ, causes increase of the SERR.

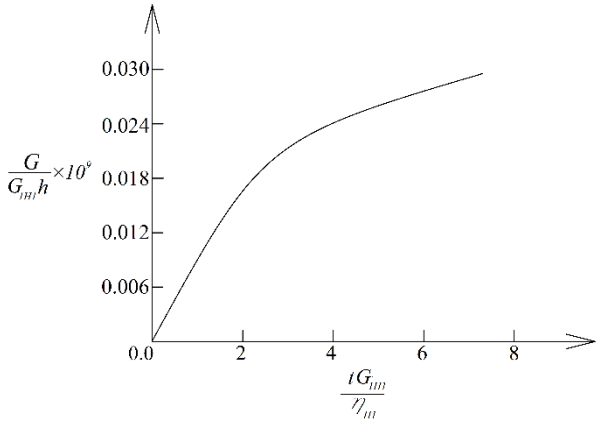

Fig. 4 The SERR presented as a function of time

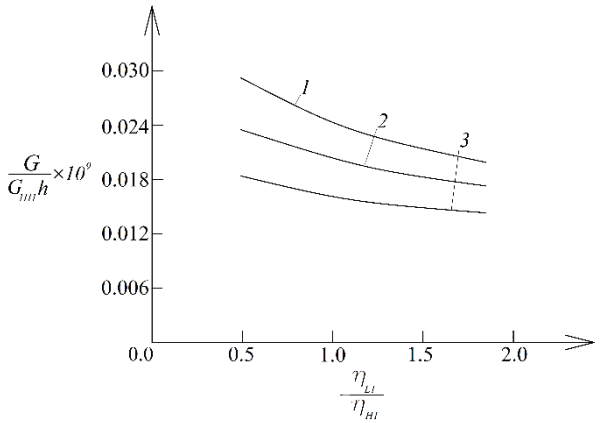

Fig. 5 The SERR presented as a function of η_{L1}/η_{H1} ratio (curve 1 - at G_{2L1}/G_{2H1}=0.5, curve 2 - at G_{2L1}/G_{2H1}=1.0 and curve 3 - at G_{2L1}/G_{2H1}=2.0)

The evolution of the SERR with time is presented in Fig. 4. Time in Fig. 4 is expressed in non-dimensional form as $t_N = tG_{1H1}/\eta_{H1}$.

The influence of variations of η_1 and G_{21} in longitudinal direction of beam layer 1 on the SERR is analyzed too. The results of the analysis are illustrated in Fig. 5 where the SERR is presented as a function of η_{L1}/η_{H1} at three G_{2L1}/G_{2H1} ratios. Fig. 5 shows that the SERR reduces when η_{L1}/η_{H1} ratio increases. The inspection of Fig. 5 indicates that increase of G_{2L1}/G_{2H1} ratio induces also reduction of the SERR.

One can examine the effect of the ratios of the properties in layer 2 and layer 1 in Fig. 6 where the variation of the SERR with increase of G_{1H2}/G_{1H1} ratio is presented at three G_{2H2}/G_{2H1} ratios. The curves in Fig. 6 indicate that the SERR reduces with increasing of G_{1H2}/G_{1H1} and G_{2H2}/G_{2H1} ratios.

The effect of the ratio of the coefficients of viscosity in layer 3 and layer 1 on the SERR is also analyzed. The dependency obtained is plotted in Fig. 7. One can observe in Fig. 7 that increase of η_{H3}/η_{H1} ratio generates reduction of the SERR. It can also be observed in Fig. 7 that the SERR derived at increase of the delamination length at delamination tip located in beam section, R_4, is

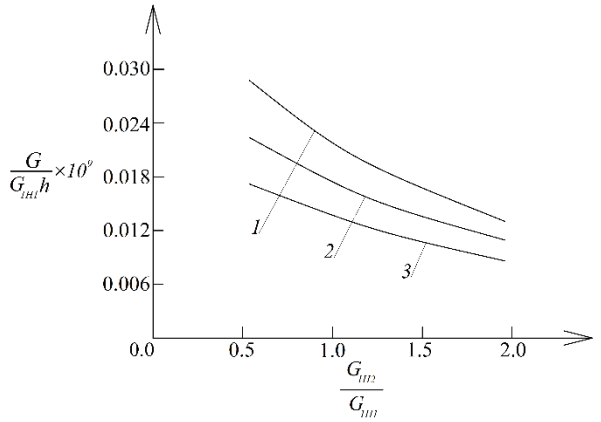

Fig. 6 The SERR presented as a function of G_{1H2}/G_{1H1} ratio (curve 1 - at G_{2H2}/G_{2H1}=0.5, curve 2 - at G_{2H2}/G_{2H1}=1.0 and curve 3 - at G_{2H2}/G_{2H1}=2.0)

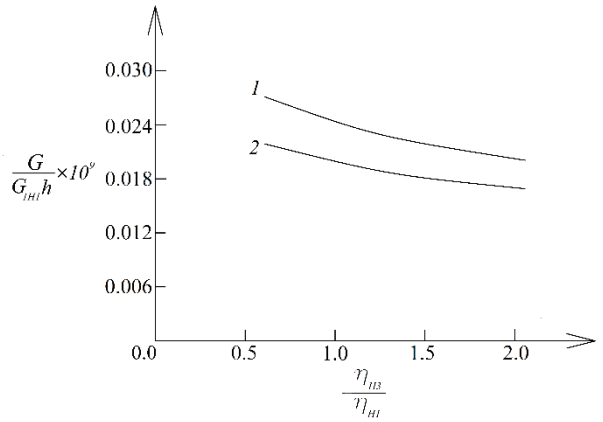

Fig. 7 The SERR presented as a function of η_{H3}/η_{H1} ratio (curve 1 - at increase of the delamination length at delamination tip located in beam section, R_3, and curve 2 - at increase of the delamination length at delamination tip located in beam section, R_4)

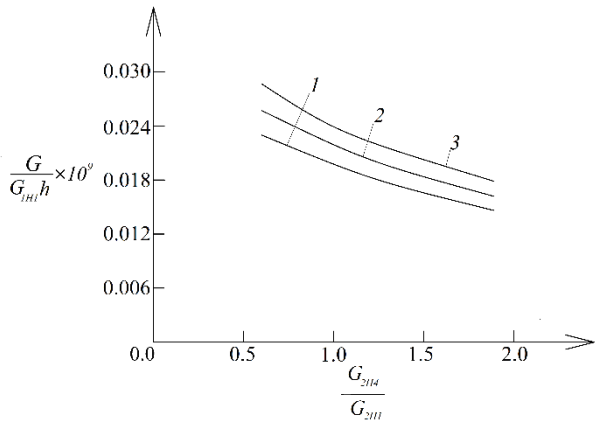

Fig. 8 The SERR presented as a function of G_{2H4}/G_{2H1} ratio (curve 1 - at a_1/l_1=0.3, curve 2 - at a_1/l_1=0.5 and curve 3 - at a_1/l_1=0.7)

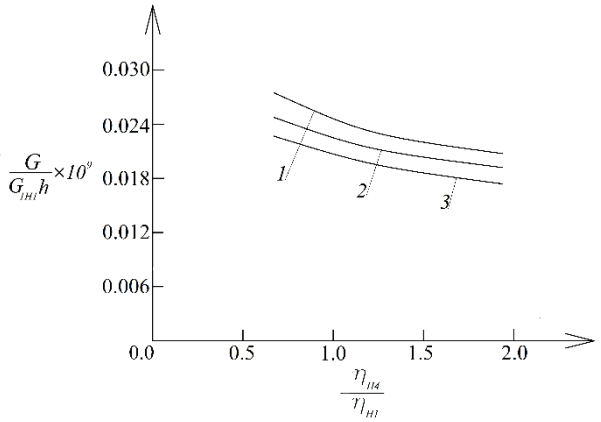

Fig. 9 The SERR presented as a function of η_{H4}/η_{H1} ratio (curve 1 - at $a_2/(l-l_1)$=0.3, curve 2 - at $a_2/(l-l_1)$=0.5 and curve 3 - at $a_2/(l-l_1)$=0.7)

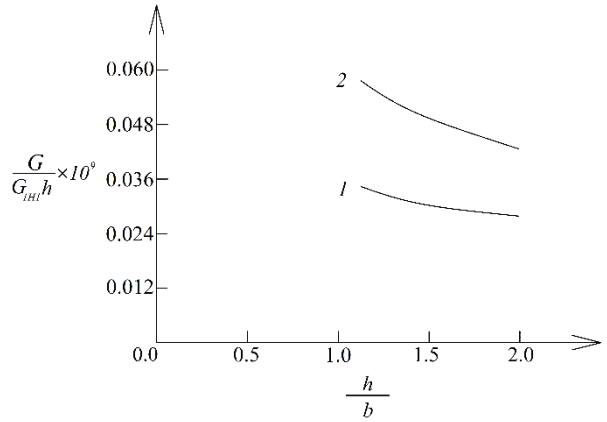

Fig. 10 The SERR presented as a function of *h*/*b* ratio (curve 1 - under pure torsion and curve 2 - under torsion and bending)

lower than that found at increase at the delamination tip located in beam section, R_3 (this caused by the fact that the material properties in section, R_4, of the beam have higher values than in the beam section, R_3, since the material properties values increase from the free end of the beam towards the clamped end.

The influence of the a_1/l_1 ratio on the SERR is investigated. The dependency of the SERR on a_1/l_1 and G_{2H4}/G_{2H1} ratios is displayed in Fig. 8. One can observe in Fig. 8 that when a_1/l_1 ratio increases, the SERR increases too. The increase of G_{2H4}/G_{2H1} ratio generates reduction of the SERR (Fig. 8).

The variation of the SERR with increase of $a_2/(l-l_1)$ and η_{H4}/η_{H1} ratios is displayed in Fig. 9. The analysis of the curves in Fig. 9 reveals that the SERR reduces with increase of $a_2/(l-l_1)$ and η_{H4}/η_{H1} ratios. In this case, the reduction of the SERR with increase of $a_2/(l-l_1)$ ratio is due to the fact that the delamination tip, R_4, changes its position in direction of increase of the values of material properties (the material properties and the beam stiffness increase from the free end towards the clamped end of the beam).

Delamination analysis with bending-torsion coupling is also performed. The bending response of the multilayered inhomogeneous beam under strain-path control is treated through a viscoelastic model that has the same schematic as this depicted in Fig. 1 by replacing of γ_j, η_j, G_{1j} and G_{2j} with ε_j, η_{Lj}, E_{1j} and E_{2j}, respectively (here, ε_j is the linear strain induced by the bending, η_{Lj} is the coefficient of viscosity, E_{1j} and E_{2j} are the moduli of elasticity of the two springs in the model). The same replacements are carried-out in Eqs. (3), (4) and (6) for obtaining of the time-dependent modulus of elasticity, E_{Dj}, that is applied in the delamination analysis under bending. Analogical replacements are performed in Eqs. (8), (9) and (10) for describing the distributions of E_{1j}, E_{2j} and η_{Lj} along the length of the beam. The static indeterminacy of the beam loaded in bending is resolved by applying the theorem of Menabrea. The SERR, G_L, due to bending of the beam under strain-path control is found-out by using Eq. (37) for the delamination tip in section, R_2, where the strain energy densities are determined through replacement of τ_j and G_{Dj} with σ_j and E_{Dj} in Eq. (16). Here, σ_j is the normal stress induced by bending of the beam. Similar replacements are conducted in Eq. (39) to derive the SERR (due to bending of the beam under strain-path control) for the delamination tip located in section, R_2. The solutions of the SERR are verified by analyzing the beam compliance under bending. The total SERR, G_{LT}, due to bending-torsion coupling is determined by addition of G and G_L, i.e., $G_{LT}=G+G_L$.

The outcome of the delamination analysis with bending-torsion coupling is compared with the torsion case alone in Fig. 10. One can see that bending-torsion coupling causes a substantial growth of the SERR in comparison with the torsion alone (Fig. 10).

5. Conclusions

Delamination in a multilayered inhomogeneous beam configuration with rectangular cross-section loaded in torsion under strain-path control is analyzed with taking into account the viscoelastic behavior of the material. Solution of the SERR is obtained. The main findings are formulated as:

- the SERR increases with increasing of the parameter, ν_φ,
- the increase of G_{1L1}/G_{1H1}, η_{L1}/η_{H1}, G_{2L1}/G_{2H1}, G_{1H2}/G_{1H1}, G_{2H2}/G_{2H1}, η_{H3}/η_{H1}, G_{2H4}/G_{2H1} and η_{H4}/η_{H1} ratios causes reduction of the SERR,
- the SERR obtained at increase of the delamination length at delamination tip located in beam cross-section, R_4, is lower than that determined at increase at the delamination tip located in beam cross-section, R_3,
- the SERR reduces with increase of $a_2/(l-l_1)$ ratio,
- the SERR grows with increase of a_1/l_1 ratio,
- bending-torsion coupling causes a substantial growth of the SERR in comparison with the torsion case alone.

References

Ahmed, R.A., Fenjan, R.M., Hamad, L.B. and Faleh, N.M. (2020), "A review of effects of partial dynamic loading on dynamic response of nonlocal functionally graded material beams", *Adv. Mater. Res.*, **9**(1), 33-48. https://doi.org/10.12989/amr.2020.9.1.033.

Akbulut, M. and Sonmez, F.O. (2008), "Optimum design of composite laminates for minimum thickness", *Comput. Struct*., **86**(21-22), 1974-1982. https://doi.org/10.1016/j.compstruc.2008.05.003.

Akbulut, M., Sarac, A. and Ertas, A.H. (2020), "An investigation of non-linear optimization methods on composite structures under vibration and buckling loads", *Adv. Comput. Des.*, **5**, 209-231. https://doi.org/10.12989/acd.2020.5.3.209 209.

Butcher, R.J., Rousseau, C.E. and Tippur, H.V. (1999), "A functionally graded particulate composite: Measurements and Failure Analysis", *Acta. Mater.*, **47**(2), 259-268. https://doi.org/10.1016/S1359-6454(98)00305-X.

Carpinteri, A. and Pugno, N. (2006), "Cracks in re-entrant corners in functionally graded materials", *Eng. Fract. Mech.*, **73**, 1279-1291. https://doi.org/10.1016/j.engfracmech.2006.01.008.

Chen, F., Jia, M., She, Y., Wu, Y., Shen, Q. and Zhang, L. (2020), "Mechanical behavior of AlN/Mo functionally graded materials with various compositional structures", *J. Alloys. Compd.*, **816**, 152512. https://doi.org/10.1016/j.jallcom.2019.152512.

Chobanian, K.S. (1997), *Stresses in Combined Elastic Solids*, Science.

Dolgov, N.A. (2002), "Effect of the elastic modulus of a coating on the serviceability of the substrate-coating system", *Strength Mater.*, **34**, 153-157. https://doi.org/10.1023/A:1015362426688.

Dolgov, N.A. (2005), "Determination of stresses in a two-layer coating", *Strength Mater.*, **37**(2), 422-431. https://doi.org/10.1007/s11223-005-0053-7.

Dolgov, N.A. (2016), "Analytical methods to determine the stress state in the substrate-coating system under mechanical loads", *Strength Mater.*, **48**(1), 658-667. https://doi.org/10.1007/s11223-016-9809-5.

Gasik, M.M. (2010), "Functionally graded materials: Bulk processing techniques", *Int. J. Mater. Prod. Technol.*, **39**(1-2), 20-29. https://doi.org/10.1504/IJMPT.2010.034257.

Hedia, H.S., Aldousari, S.M., Abdellatif, A.K. and Fouda, N.A. (2014), "New design of cemented stem using functionally graded materials (FGM)", *Biomed. Mater. Eng*., **24**(3), 1575-1588. https://doi.org/10.3233/BME-140962.

Hirai, T. and Chen, L. (1999), "Recent and prospective development of functionally graded materials in Japan", *Mater. Sci. Forum*, **308-311**(4), 509-514. https://doi.org/10.4028/www.scientific.net/MSF.308-311.509.

Hsueh, C.H., Tuan, W.H. and Wei, W.C.J. (2006), "Analyses of steady-state interface fracture of elastic multilayered beams under four-point bending", *Scripta Mater.*, **60**, 721-724. https://doi.org/10.1016/j.scriptamat.2009.01.001.

Hutchinson, J.W. and Suo, Z. (1992), "Mixed mode cracking in layered materials", *Adv. Appl. Mech.*, **64**, 804-810. https://doi.org/10.1016/S0065-2156(08)70164-9.

Madan, R., Saha, K. and Bhowmick, S. (2020), "Limit speeds and stresses in power law functionally graded rotating disks", *Adv. Mater. Res.*, **9**(2), 115-131. https://doi.org/10.12989/amr.2020.9.2.115.

Mahamood, R.M. and Akinlabi, E.T. (2017), *Functionally Graded Materials*, Springer International Publishing, Cham, Switzerland.

Markworth, A.J., Ramesh, K.S. and Parks, Jr.W.P. (1995), "Review: Modeling studies applied to functionally graded materials", *J. Mater. Sci.*, **30**(3), 2183-2193. https://doi.org/10.1007/BF01184560.

Miyamoto, Y., Kaysser, W.A., Rabin, B.H., Kawasaki, A. and Ford, R.G. (1999), *Functionally Graded Materials: Design, Processing and Applications*, Springer, New York, NY, USA.

Nemat-Allal, M.M., Ata, M.H., Bayoumi, M.R. and Khair-Eldeen, W. (2011), "Powder metallurgical fabrication and microstructural investigations of aluminum/steel functionally graded material", *Mater. Sci. Appl.*, **2**(5), 1708-1718. https://doi.org/10.4236/msa.2011.212228.

Nguyen, S.N., Lee, J. and Cho, M. (2015), "Efficient higher-order zig-zag theory for viscoelastic laminated composite plates", *Int. J. Solids Struct.*, **62**, 174-185. https://doi.org/10.1016/j.ijsolstr.2015.02.027.

Nguyen, S.N., Lee, J., Han, J.W. and Cho, M. (2020), "A coupled hygrothermo-mechanical viscoelastic analysis of multilayered composite plates for long-term creep behaviors", *Compos. Struct.*, **242**, 112030. https://doi.org/10.1016/j.compstruct.2020.112030.

Nikbakht, S., Kamarian, S. and Shakeri, M.A. (2019), "A review on optimization of composite structures Part II: Functionally graded materials", *Compos. Struct.*, **214**, 83-102.

https://doi.org/10.1016/j.compstruct.2019.01.105.
Radhika, N., Sasikumar, J., Sylesh, J.L. and Kishore, R. (2020), "Dry reciprocating wear and frictional behaviour of B4C reinforced functionally graded and homogenous aluminium matrix composites", *J. Mater. Res. Technol.*, **9**, 1578-1592. https://doi.org/10.1016/j.jmrt.2019.11.084.
Rizov, V. (2023), "Delamination analysis of multilayered functionally graded beams which exhibit non-linear creep behavior", *J. Appl. Comput. Mech*., **9**(4), 935-944 https://doi.org/10.22055/jacm.2023.42743.3969.
Rizov, V.I. (2018), "Non-linear fracture in bi-directional graded shafts in torsion", *Multidiscip. Model. Mater. Struct.*, **14**, 387-399. https://doi.org/10.1108/MMMS-12-2017-0163.
Rizov, V.I. (2020), "Longitudinal fracture analysis of continuously inhomogeneous beam in torsion with stress relaxation", *Struct. Integr. Proc.*, **28**, 1212-122. https://doi.org/10.1016/j.prostr.2020.11.103.
Rizov, V.I. (2021), "Delamination analysis of multilayered beams exhibiting creep under torsion", *Coupl. Syst. Mech.*, **10**, 317-331. https://doi.org/10.12989/csm.2021.10.4.317.
Rizov, V.I. (2022), "Effects of periodic loading on longitudinal fracture in viscoelastic functionally graded beam structures", *J. Appl. Comput. Mech*., **8**(1), 370-378. https://doi.org/10.22055/JACM.2021.37953.3141.
Rizov, V.I. and Altenbach, H. (2023), "Fracture analysis of inhomogeneous arch with two longitudinal cracks under non-linear creep", *Adv. Mater. Res.*, **12**(1), 15-29. https://doi.org/10.12989/amr.2023.12.1.015.
Saiyathibrahim, A., Subramanian, R. and Samson Jerold Samuel, C. (2019), "Processing and properties evaluation of centrifugally cast *in-situ* functionally graded composites reinforced with Al_3Ni and Si particles", *Mater. Res. Express*, **6**(11) 1165a8. https://doi.org/10.1088/2053-1591/ab4c9f.
Shrikantha Rao, S. and Gangadharan, K.V. (2014), "Functionally graded composite materials: An overview", *Proc. Mater. Sci.*, **5**(1), 1291-1299. https://doi.org/10.1016/j.mspro.2014.07.442.
Tilbrook, M.T., Moon, R.J. and Hoffman, M. (2005), "Crack propagation in graded composites", *Compos. Sci. Technol.*, **65**, 201-220. https://doi.org/10.1016/j.compscitech.2004.07.004.
Toudehdehghan, J., Lim, W., Foo, K.E., Ma'arof, M.I.N. and Mathews, J. (2017), "A brief review of functionally graded materials", *MATEC Web Conf.*, **131**, 03010. https://doi.org/10.1051/matecconf/201713103010.
Uslu Uysal, M. (2016), "Buckling behaviours of functionally graded polymeric thin-walled hemispherical shells", *Steel Compos. Struct.*, **21**(1), 849-862. https://doi.org/10.12989/scs.2016.21.4.849.
Uslu Uysal, M. and Güven, U. (2015), "Buckling of functional graded polymeric sandwich panel under different load cases", *Compos. Struct.*, **121**, 182-196. https://doi.org/10.1016/j.compstruct.2014.11.012.
Uslu Uysal, M. and Güven, U. (2016), "A bonded plate having orthotropic inclusion in adhesive layer under in-plane shear loading", *J. Adhes.*, **92**, 214-235. https://doi.org/10.1080/00218464.2015.1019064.
Uslu Uysal, M. and Kremzer, M. (2015), "Buckling behaviour of short cylindrical functionally gradient polymeric materials", *Acta Phys. Polon.*, **A127**, 1355-1357. https://doi.org/10.12693/APhysPolA.127.1355.
Zubchaninov, V.G. (1990), *Fundamentals of Theory of Elasticity and Plasticity*, Vishaya Shcola, Minsk, Belarus.

CC